IOP Publishing Physica Scripta
Phys. Scr. 95 (2020) 045207 (17pp) https://doi.org/10.1088/1402-4896/ab5ca7

Bioconvection of Maxwell nanofluid under the influence of double diffusive Cattaneo–Christov theories over isolated rotating disk

S A Shehzad[1,4], M G Reddy[2], A Rauf[1,3] and Z Abbas[3]

[1] Department of Mathematics, COMSATS University Islamabad, Sahiwal Campus, 57000, Pakistan
[2] Department of Mathematics, Acharya Nagarjuna University Campus, Ongole-523001, A.P., India
[3] Department of Mathematics, The Islamia University of Bahawalpur, Bahawalpur, 63100, Pakistan

E-mail: ali_qau70@yahoo.com

Received 19 October 2019, revised 26 November 2019
Accepted for publication 28 November 2019
Published 12 February 2020

Abstract

An incompressible, MHD, bioconvective flow of Maxwell fluid is studied. The rotating isolated disk caused the fluid motion. The disk also stretches with constant rate along radial direction. Cattaneo–Christov energy and mass species flux models are adopted. Buongiorno model of nanofluid is executed in the constitutive equations along with gyrotactic microorganisms. The transformation of Von-Karman assist to obtained nonlinear system of ordinary differential equations. The final controlled equations are resolved by adopting Runge–Kutta–Fehlberg numerical procedure. Graphical illustrations of results are accounted. It is percieved that velocity field is reduced by velocity ratio parameter. themphoretic, Brownian motion and thermal relaxation time parameters enhanced thermal fields respectively. Motile organisms rate is declined due to bioconvection Peclet number.

Keywords: rotating disk, Maxwell nanofluid, gyrotactic microorganisms, Cattaneo–Christov theories, magnetohydrodynamic

(Some figures may appear in colour only in the online journal)

1. Introduction

The non-Newtonian liquid flows across a rotating disk is very prominent and emerging area of research in the recent days due a wide applications of industrial and mechanical engineering, which include production of petroleum processes, production of polymer sheet food processing in advanced technology, electric and turbo power generating system analysis. Based on the above mentioned inspired applications, the mathematical flow in a rotating disk was originally studied by Karman [1]. After his pioneer contribution, the hydro-dynamical liquid flow in a two-dimensional (2D) rotational disk has been discussed numerically by Cochran [2]. Thermal analysis due to a rotational disk was addressed by Millsaps and Pohlhausen [3]. Acrivos *et al* [4] have described the governing flow equations on the non-Newtonian fluid across a rotating disk in 1960. The 2D rotating disk flow in a non-Newtonian liquid was studied by Jain [5]. He employed the second-order velocity strain–stress relations in classical hydrodynamics. The power-law liquid flow analysis induced by a rotating disk was reported by Andersson *et al* [6]. They utilized the similarity transformations for simplifying the governing modeled equations. Attia [7] considered the heat transfer on non-Newtonian flow induced by disk rotation. He obtained the exact solutions for velocity and temperature. The heat transfer and numerical simulation on Burgers' liquid along an eccentric rotating stretchable disks was emphasized by Siddiqui *et al* [8]. Tabassum Mustafa [9] have considered the numerical heat transfer flow on non-Newtonian Reiner-Rivlin fluid. Exploration of variable thermal conductivity on swirling hydrodynamic heat flow in Maxwell fluid induced by two rotating disks have been addressed very recently by Ahmed *et al* [10]. They

[4] Author to whom any correspondence should be addressed.

emphasized that the energy profile is increased for the magnetic field parameter. Some researches induced by disk rotation have been reported in [11–15].

In recent era, multiple efforts are made to execute the real behavior of nanofluids. The regular heat transportation fluids like water, ethanediol and engine oil have weaker abilities of energy transport because of their lesser thermal conductivity. The insertion of higher thermal conductive metal-particles in regular energy transport fluid may improve the thermal efficiency of the resulting fluid. The term 'Nanofluid' has been recommended by Choi [16]. Thermal conductivity is the most outstanding feature of nanofluid which makes its more effective and suitable for the present technological and industrial processes [17]. Turkyilmazoglu [18] executed the energy transport phenonmenon of nanofluid flow generated by disk rotation. Hayat *et al* [19] studied the thermophoresis and Brownian motion impacts in second grade fluid flow subject to rotating disk. Hayat *et al* [20] analyze the statistical declartion for two phase radiative flow confined throgh stretchable disks and computed probable error. They scrutinazed that at disks surfaces, the drag force is less aganist rotational parameter. Analytical approach using HAM is adopted to discussed thermal features of third grade nanofluid flow via stretchable disk by Hayat *et al* [21]. They contributed to the fact that concentration as well as temperature enhanced with Brownian motion and velocity is reduced by material parameters. Ahmad *et al* [22] presented the entropy analysis of viscous squeezign flow of two sheets by considering five distinct configurations of nanoparticles. They found that nanoparticles volume fraction enhanced entropy generation. Three dimensional (3D) flow of hydromagnetic nanofluid examined by Aziz *et al* [23]. They obtained the solution with the aid of ND solve technique with Matlab software. It is worthy noticed that as the boosting values of thermophoresis exhibits uniform trend in the both concentration and temperature. Mahanthesh *et al* [24] numerically scrutinized thermal attributes of distinct shapes nanoparticles in radiative viscous fluid flow caused by a rotating disk. Sheikholeslami and Shehzad [25] estimated the nanofluid characteristics in convective flow through porous enclosure using CVFEM technique. RK-4 method was adopted to discuss the hall current attributes of hybrid nanofluid flow through spinning isolated disk by Acharya *et al* [26]. It is established that the Hall influence escalated the radial velocity and declines temperature field. Mehmood *et al* [27] modeled the combined heat and species transfer analysis over a rotating wavy disk. Stagnation Maxwell nanoliquid flow has been investigated by Jawad *et al* [28].

The energy transfer mechanism was reported by Fourier law [29] of heat conduction theory. The heat transport mechanism having a plenty number of engineering applications which include like the nuclear-reactor cooling, heat conduction in production systems, drug delivery and targeting in medical treatment. The Cattaneo–Christov (C–C) heat flux on Jeffrey fluid flow has been explored by Hayat *et al* [30]. Scrutinization of C–C heat diffusion flow over thicked surface has been made by Hayat *et al* [31]. Mustafa [32] analyzed the energy transfer in Maxwell fluid under C–C heat diffusion formula. Reddy *et al* [33, 34] have employed this theory on thermal radiative flows of Oldroyd-B fluid over wedge/cone. Abbasi and Shehzad [35] discussed the energy transfer on 3D Maxwell fluid by employing C–C heat flux theory. Shehzad *et al* [36] demonstrated the C–C heat flux model for rate type flows of non-Newtonian materials.

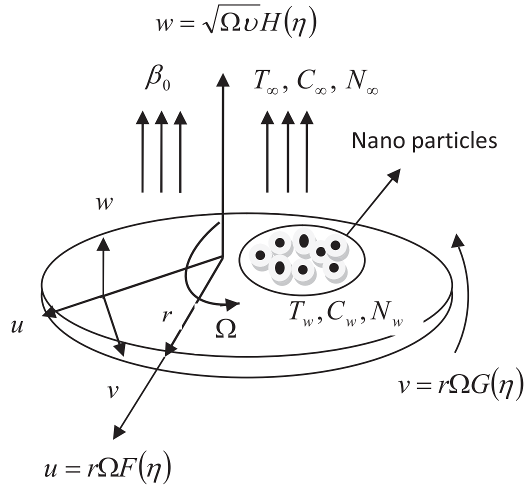

Figure 1. Flow configuration.

Nanofluids have upgraded thermophysical characteristics such as thermal diffusivity and thermal conductivity which are important in numerous industrial applications include transportation, nuclear reactor, thermosyphons, pulsating heated pipes and biomedicine. Moreover nanoparticles higher concentration that produces larger thermal resistance due to which dynamic viscosity increases. C–C double diffusion theories are utilized by considering more features to heat and mass transfer by adding heat and mass flux relaxation rate in constitutive equations, which overcome the limitations of Fourier's and Fick's laws. With all physical aspects and the above literature analysis discloses that no work occurs on of bioconvection of Maxwell nanofluid under the influence of the C–C heat flux and double diffusion. Buongiorno model of nanofluid is executed in the constitutive equations. The transformation of Von-Karman assist to obtained non-linear system of ordinary differential equations and obtained the numerical solutions by employing Runge–Kutta–Fehlberg (RKF) numerical approach. Outcomes are represented via plots and tables for the physical flow parameters of concern.

2. Problem formulation

A mathematical model of incompressible bioconvective Maxwell nanofluid flow through rotating stretchable disk with

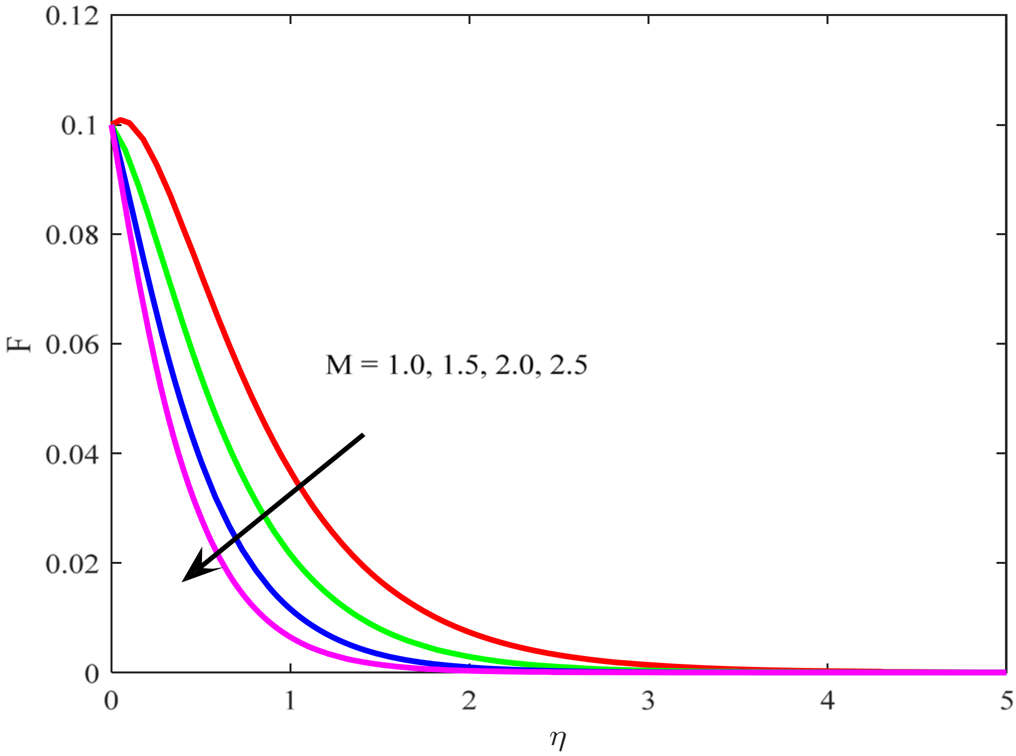

Figure 2. Behavior of M on F.

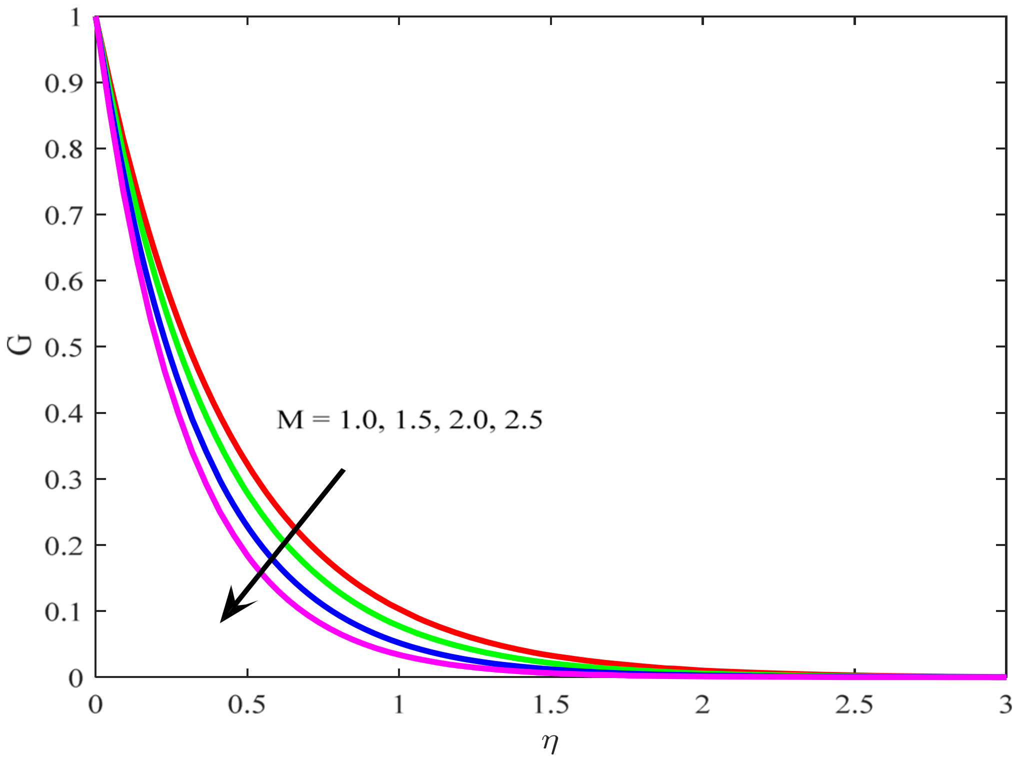

Figure 3. Behavior of M on G.

double diffusive C–C theories and magnetic field effects is considered. The isolated disk rotates with angular speed Ω and main reason to generate the fluid motion and stretches along radial direction with constant rate c. Cylindrical polar co-ordinates are the best choice considering the geometrical model. Components of velocity $(u,\ v,\ w)$ are taken in increasing directions of $(r,\ \theta,\ z)$ (see figure 1). Considering the assumption of axisymmetric flow, therefore derivatives

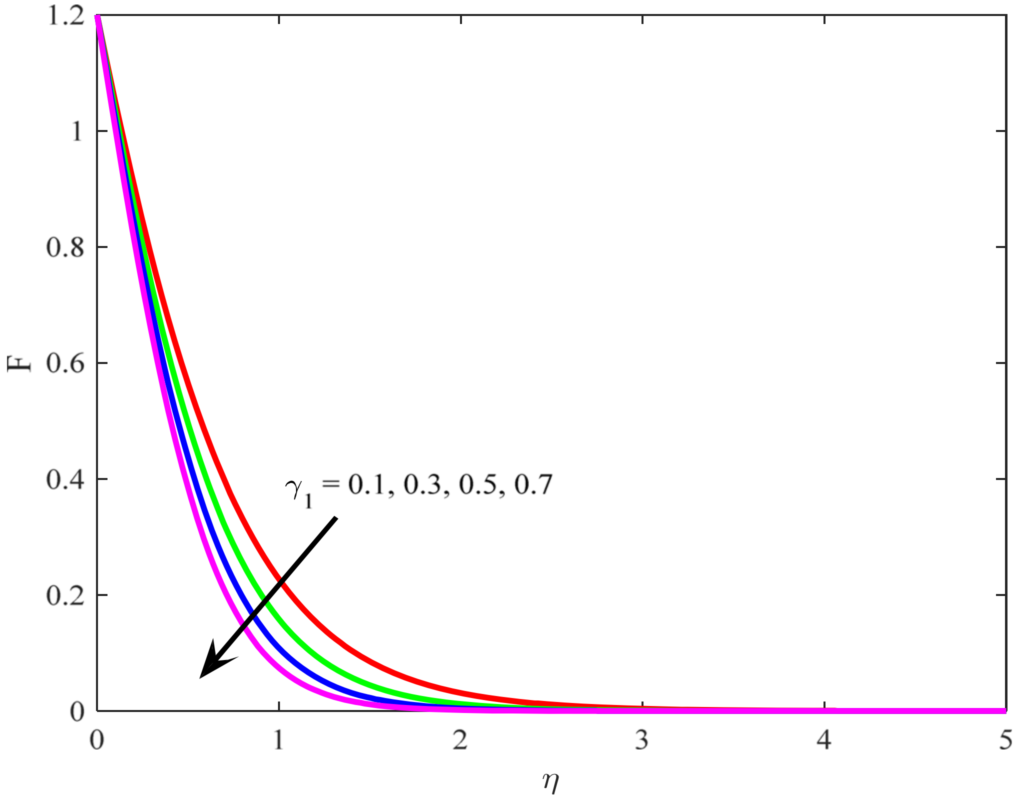

Figure 4. Behavior of γ_1 on F.

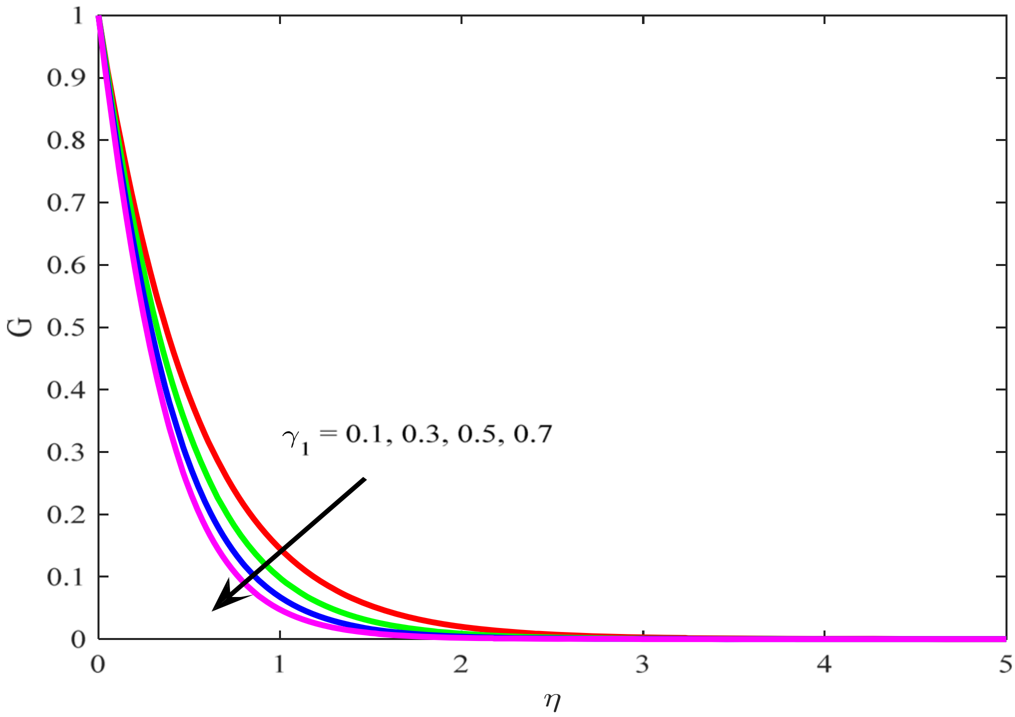

Figure 5. Behavior of γ_1 on G.

along tangential components are omitted. Electric field is overlooked due to less Reynolds number. Magnetic field having uniform potency is applied along axial direction. The disk surface temperature T_w is larger than ambient fluid temperature T_∞. The concentration at surface of disk is C_w while ambient fluid volume fraction of nanoparticles is C_∞. Microorganisms reference concentration is N_w ambient microorganisms concentration is represents by N_∞.

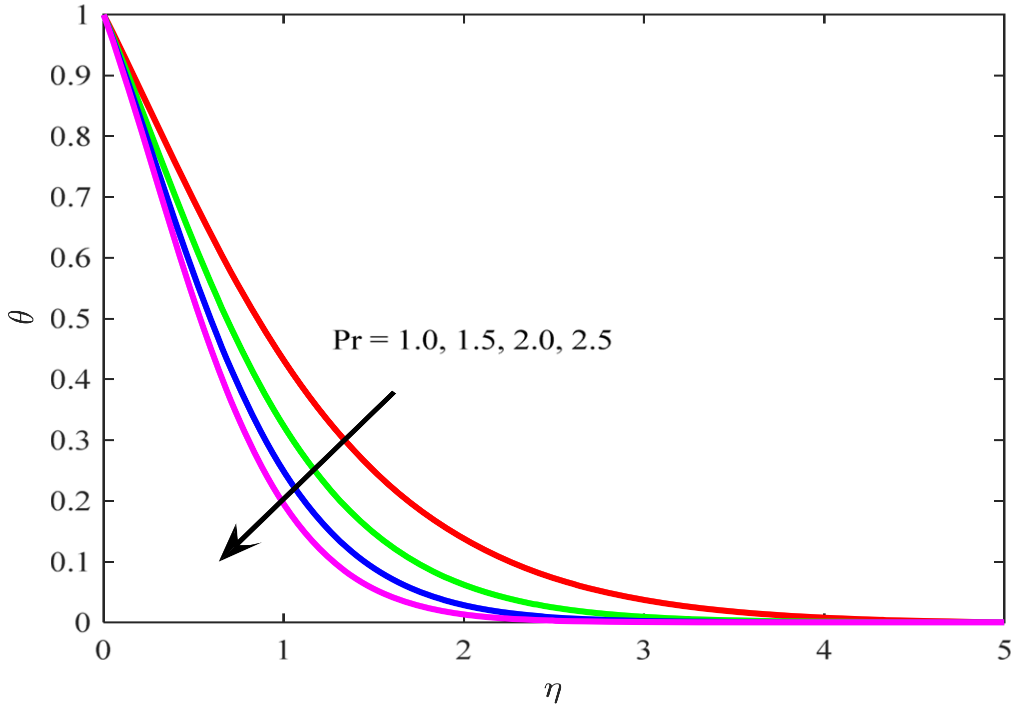

Figure 6. Behavior of Pr on θ.

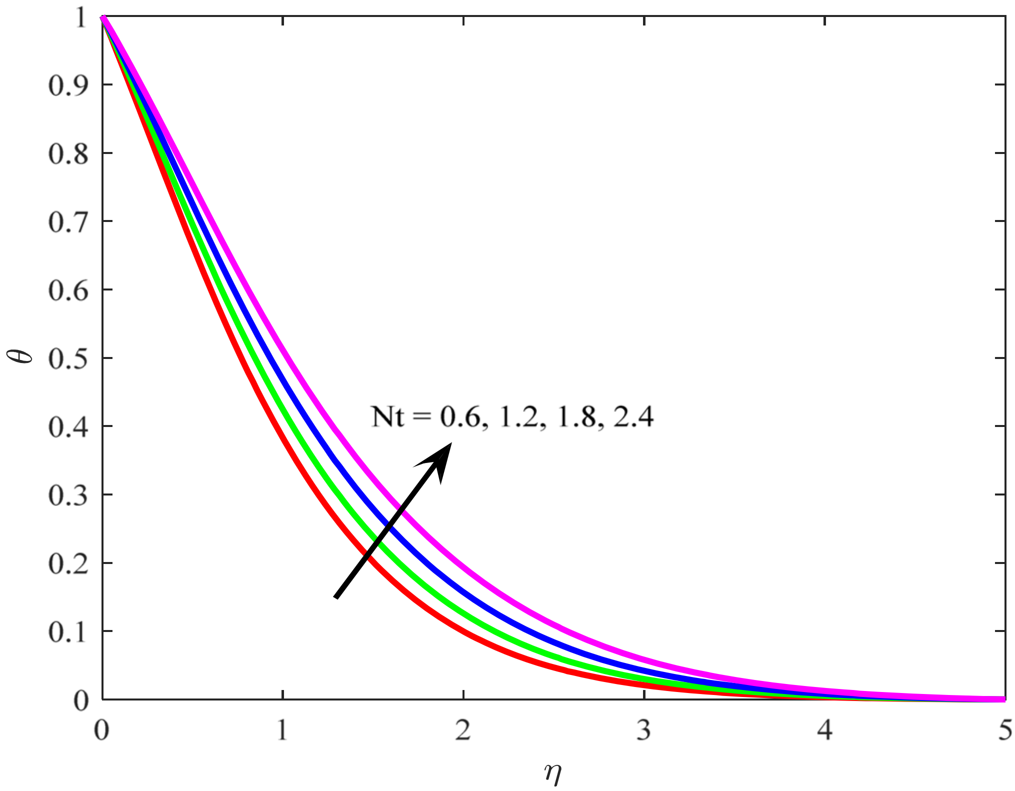

Figure 7. Behavior of Nt on θ.

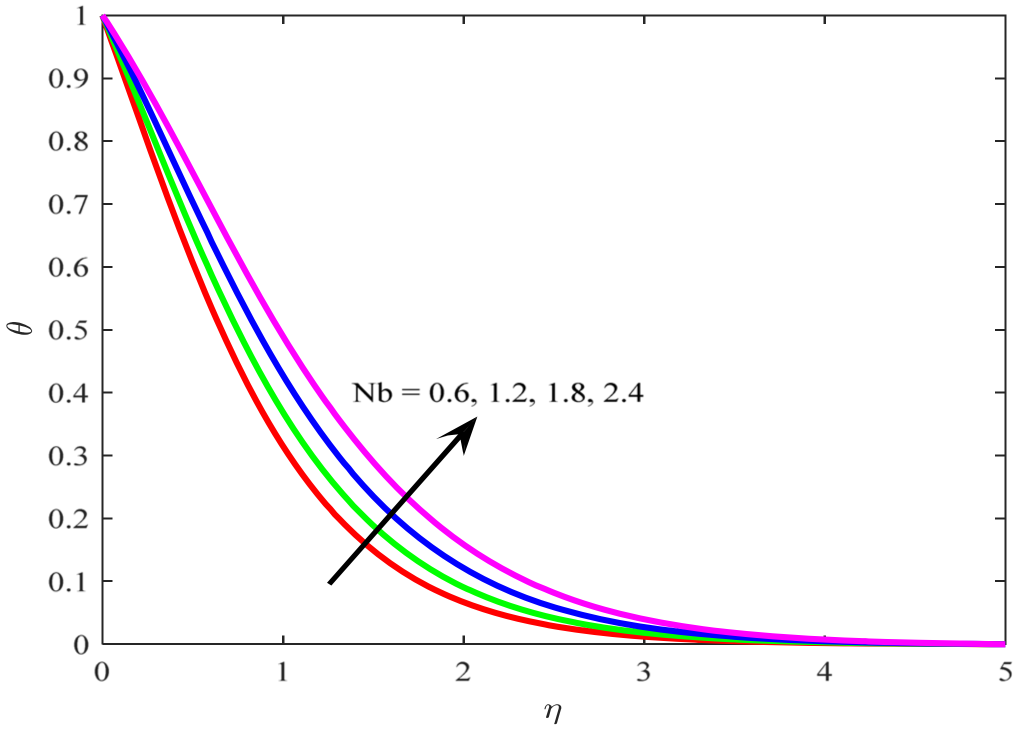

Figure 8. Behavior of Nb on θ.

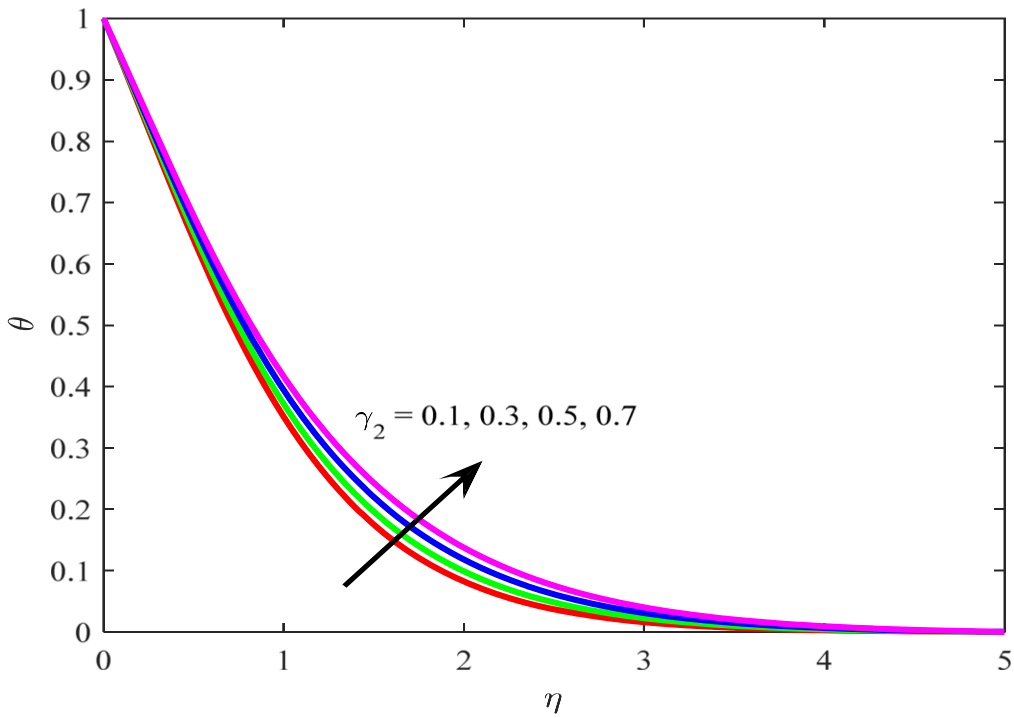

Figure 9. Behavior of γ_2 on θ.

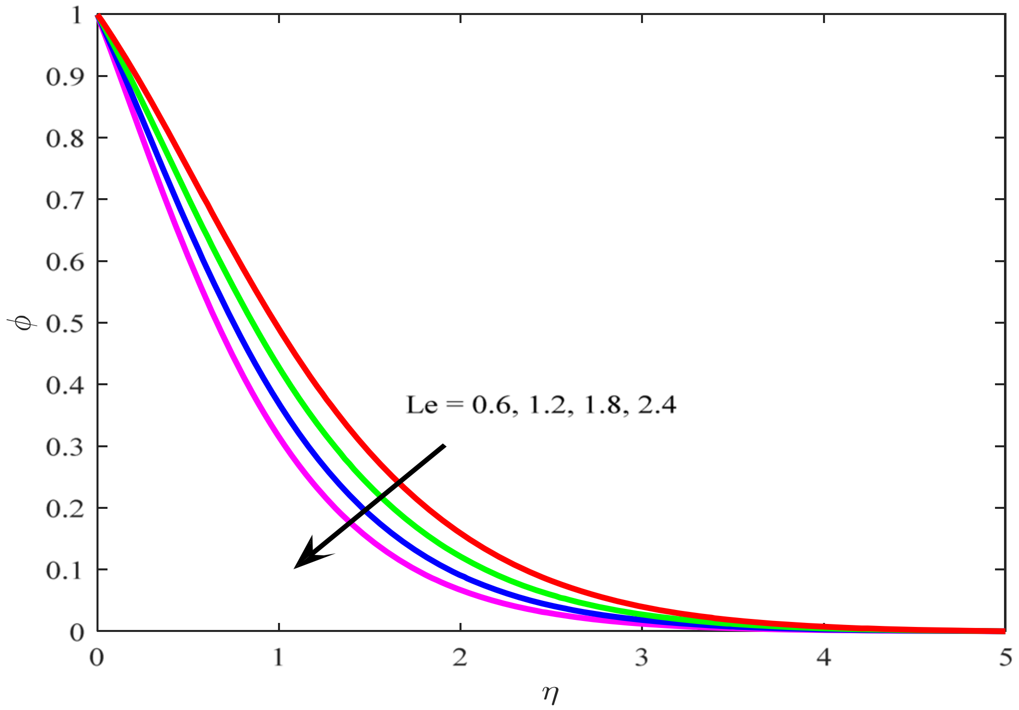

Figure 10. Behavior of *Le* on ϕ.

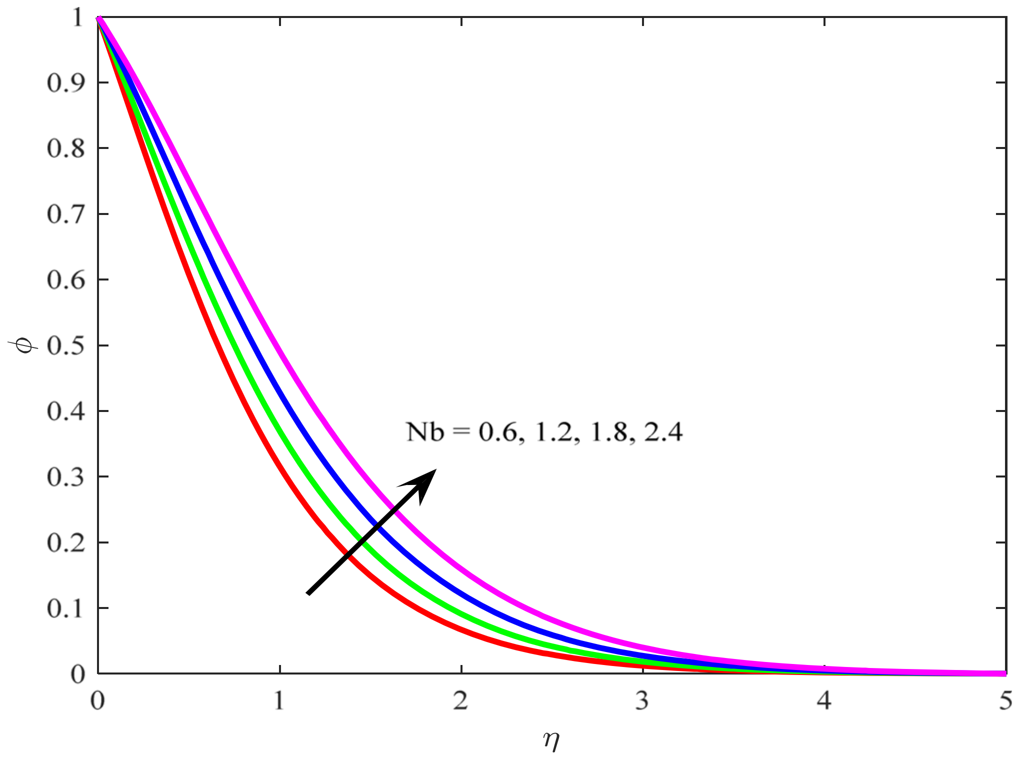

Figure 11. Behavior of *Nb* on ϕ.

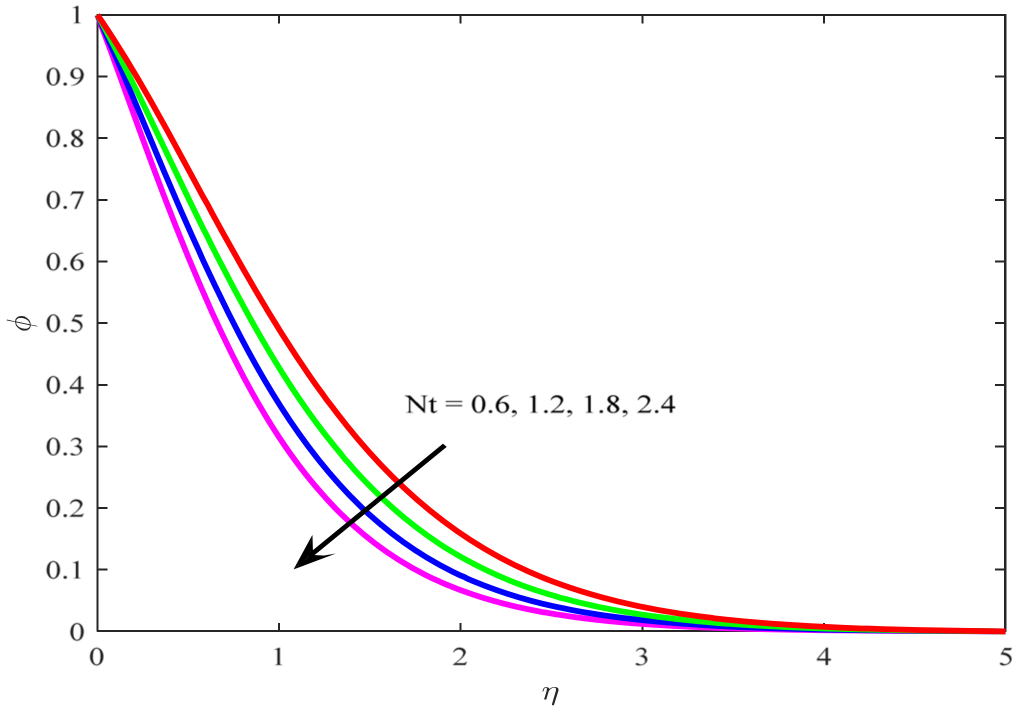

Figure 12. Behavior of Nt on ϕ.

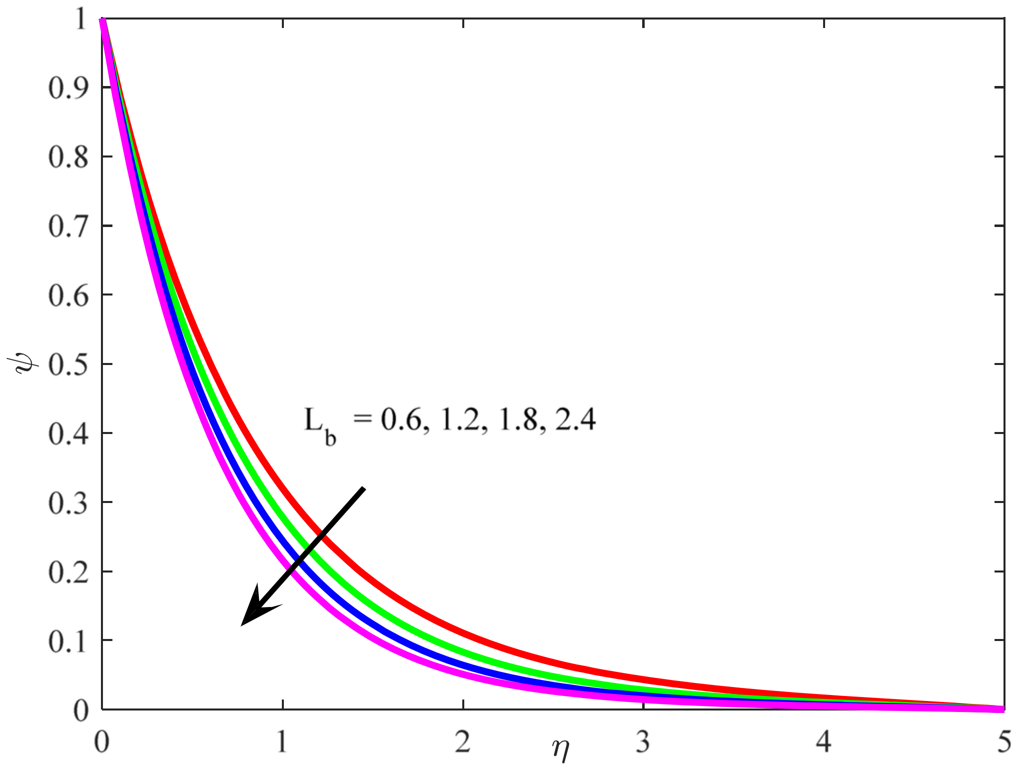

Figure 13. Impact of L_b on ψ.

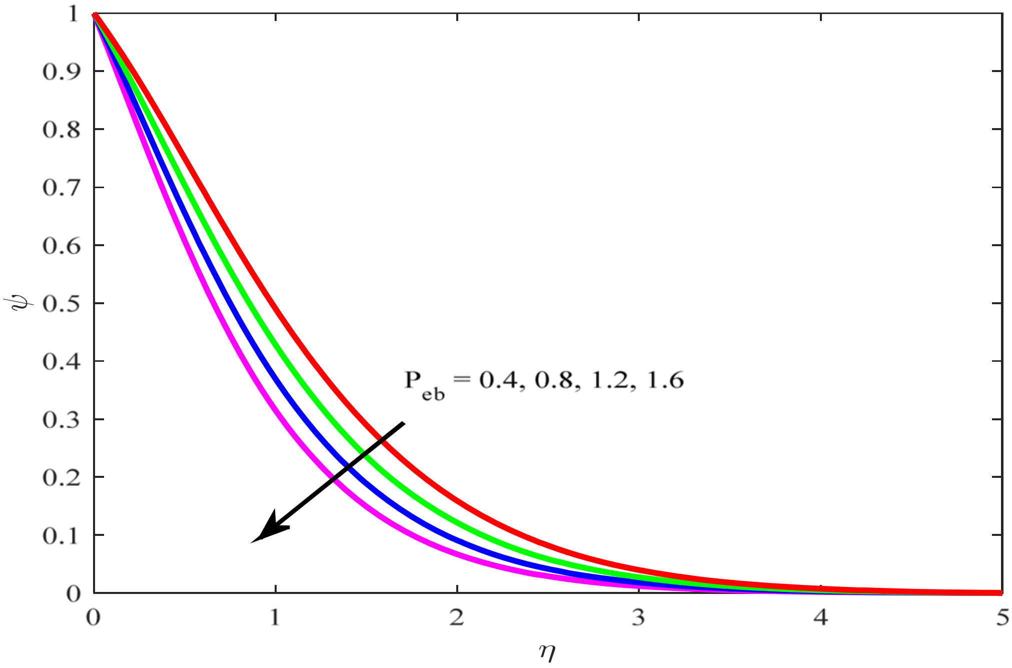

Figure 14. Behavior of P_{eb} on ψ.

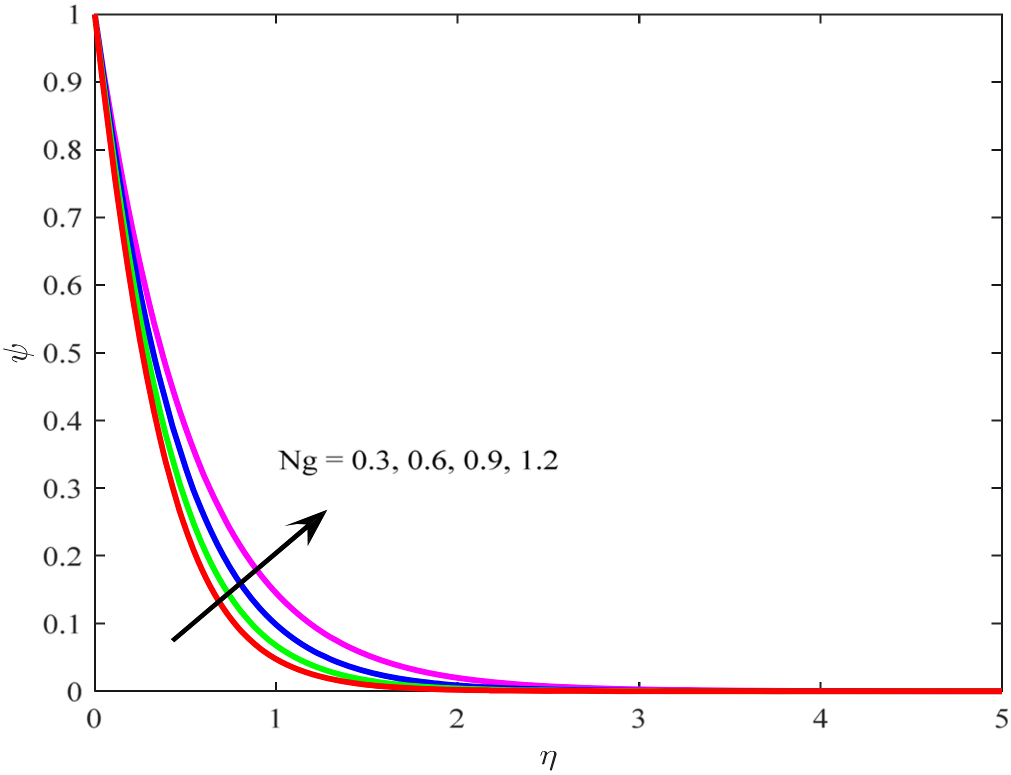

Figure 15. Behavior of Ng on ψ.

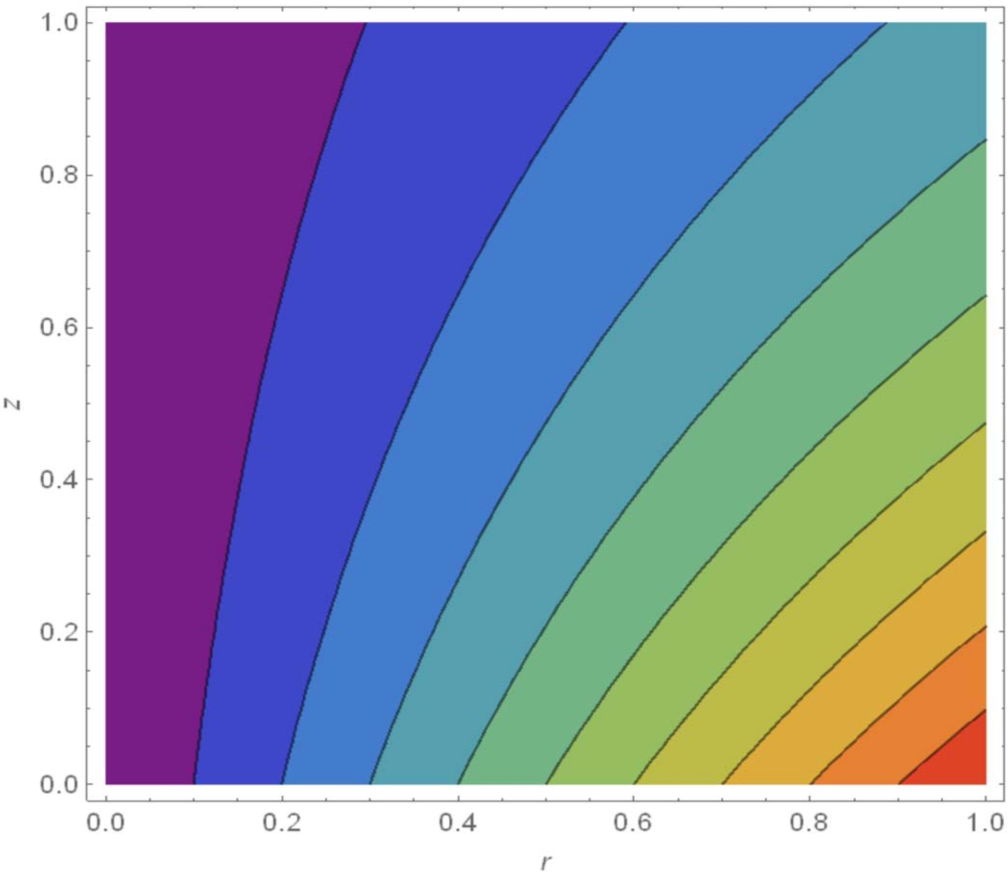

Figure 16. Stream lines for $M = 1.0$.

Governing equations in framework of above assumptions are [10, 37]:

$$\frac{\partial u}{\partial r} + \frac{u}{r} + \frac{\partial w}{\partial z} = 0, \tag{1}$$

$$u\frac{\partial u}{\partial r} + w\frac{\partial u}{\partial z} - \frac{v^2}{r} = \upsilon\left(\frac{\partial^2 u}{\partial r^2} + \frac{1}{r}\frac{\partial u}{\partial r} + \frac{\partial^2 u}{\partial z^2} - \frac{u}{r^2}\right) - \frac{\sigma_e \beta_0^2}{\rho_f}\left(u + w\lambda_1\frac{\partial u}{\partial z}\right) - \lambda_1\left(u^2\frac{\partial^2 u}{\partial r^2} + w^2\frac{\partial^2 u}{\partial z^2} + \frac{v^2}{r}\frac{\partial u}{\partial r} + 2uw\frac{\partial^2 u}{\partial r\partial z} - 2\frac{uv}{r}\frac{\partial v}{\partial r} - 2\frac{vw}{r}\frac{\partial v}{\partial z} + \frac{uv^2}{r^2}\right), \tag{2}$$

$$u\frac{\partial v}{\partial r} + w\frac{\partial v}{\partial z} + \frac{uv}{r} = \upsilon\left(\frac{\partial^2 v}{\partial r^2} + \frac{1}{r}\frac{\partial v}{\partial r} + \frac{\partial^2 v}{\partial z^2} - \frac{v}{r^2}\right) - \frac{\sigma_e \beta_0^2}{\rho_f}\left(v + w\lambda_1\frac{\partial v}{\partial z}\right) - \lambda_1\left(u^2\frac{\partial^2 v}{\partial r^2} + 2uw\frac{\partial^2 v}{\partial r\partial z} + w^2\frac{\partial^2 v}{\partial z^2} + 2\frac{uv}{r}\frac{\partial u}{\partial r} - 2\frac{u^2 v}{r^2} - \frac{v^3}{r^2} + 2\frac{vw}{r}\frac{\partial u}{\partial z} + \frac{v^2}{r}\frac{\partial v}{\partial r}\right), \tag{3}$$

$$u\frac{\partial w}{\partial r} + w\frac{\partial w}{\partial z} = -\frac{1}{\rho_f}\frac{\partial p}{\partial z} + \upsilon\left(\frac{\partial^2 w}{\partial r^2} + \frac{1}{r}\frac{\partial w}{\partial r} + \frac{\partial^2 w}{\partial z^2}\right) - \lambda_1\left(u^2\frac{\partial^2 w}{\partial r^2} + w^2\frac{\partial^2 w}{\partial z^2} + 2uw\frac{\partial^2 w}{\partial r\partial z} + \frac{v^2}{r}\frac{\partial w}{\partial r}\right), \tag{4}$$

$$u\frac{\partial T}{\partial r} + w\frac{\partial T}{\partial z} = \alpha\left(\frac{\partial^2 T}{\partial r^2} + \frac{1}{r}\frac{\partial T}{\partial r} + \frac{\partial^2 T}{\partial z^2}\right) + \tau\left(D_B\left(\frac{\partial T}{\partial r}\frac{\partial C}{\partial r} + \frac{\partial T}{\partial z}\frac{\partial C}{\partial z}\right) + \frac{D_T}{T_\infty}\left(\left(\frac{\partial T}{\partial r}\right)^2 + \left(\frac{\partial T}{\partial z}\right)^2\right)\right) - \tau_0\left(u\frac{\partial u}{\partial r}\frac{\partial T}{\partial r} + w\frac{\partial w}{\partial z}\frac{\partial T}{\partial z} + u\frac{\partial u}{\partial r}\frac{\partial T}{\partial z} + w\frac{\partial u}{\partial z}\frac{\partial T}{\partial r} - 2uw\frac{\partial^2 T}{\partial r\partial z} + u^2\frac{\partial^2 T}{\partial r^2} + w^2\frac{\partial^2 T}{\partial z^2}\right), \tag{5}$$

$$u\frac{\partial C}{\partial r} + w\frac{\partial C}{\partial z} = D_B\left(+\frac{1}{r}\frac{\partial C}{\partial r} + \frac{\partial^2 C}{\partial z^2} + \frac{\partial^2 C}{\partial r^2}\right) + \frac{D_T}{T_\infty}\left(\frac{\partial^2 T}{\partial r^2} + \frac{1}{r}\frac{\partial T}{\partial r} + \frac{\partial^2 T}{\partial z^2}\right) - \tau_1\left(u\frac{\partial u}{\partial r}\frac{\partial C}{\partial r} + w\frac{\partial w}{\partial z}\frac{\partial C}{\partial z} + u\frac{\partial u}{\partial r}\frac{\partial C}{\partial z} + w\frac{\partial u}{\partial z}\frac{\partial C}{\partial r} - 2uw\frac{\partial^2 C}{\partial r\partial z} + u^2\frac{\partial^2 C}{\partial r^2} + w^2\frac{\partial^2 C}{\partial z^2}\right), \tag{6}$$

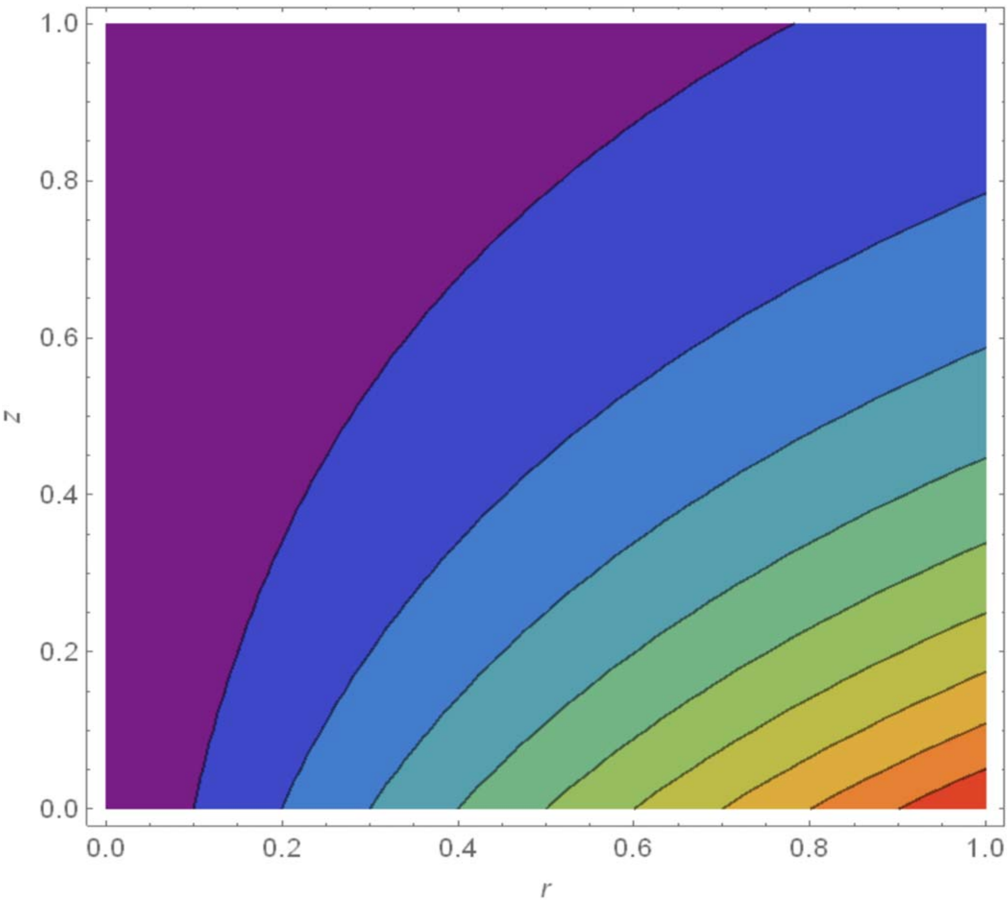

Figure 17. Stream lines for $M = 3.0$.

$$u\frac{\partial N}{\partial r} + w\frac{\partial N}{\partial z} + \left(\frac{bW_c}{C_w - C_\infty}\right)\frac{\partial N}{\partial z}\frac{\partial C}{\partial z} + N\left(\frac{bW_c}{C_w - C_\infty}\right)\frac{\partial^2 C}{\partial z^2} = D_n\left(\frac{\partial^2 N}{\partial r^2} + \frac{1}{r}\frac{\partial N}{\partial r} + \frac{\partial^2 N}{\partial z^2}\right), \tag{7}$$

with prescribed boundary conditions [37]:

$$\begin{cases} u = cr,\ v = r\Omega,\ w = 0,\ T = T_w,\ C = C_w, \\ N = N_w \text{ at } z = 0, \\ u \to 0,\ v \to 0,\ T \to T_\infty,\ C \to C_\infty, \\ N \to N_\infty \text{ as } z \to \infty. \end{cases} \tag{8}$$

Here ρ_f, υ, σ_e, β_0, λ_1, p, T, α, τ, C, D_B, D_T, τ_0, τ_1, b, N, W_c and D_n represents base fluid density and kinematic viscosity, electrical conductivity, magnetic flux density, relaxation time, pressure, temperature, thermal diffusivity of nanoparticles, ratio of nanoparticles heat capacity and base fluid, concentration, Brownian diffusion co-efficient, thermophoretic diffusion co-efficient, heat flux relaxation time, mass flux relaxation time, chemotaxis constant, microorganism, maximum cell swimming speed and microorganisms diffusion co-efficient.

Following similarity transformations are considered [10, 37]:

$$\begin{cases} u = \Omega r F(\eta),\ v = \Omega r G(\eta),\ w = \sqrt{\Omega\upsilon}\, H(\eta), \\ \theta(\eta) = \dfrac{T - T_\infty}{T_w - T_\infty}, \\ \varphi(\eta) = \dfrac{C - C_\infty}{C_w - C_\infty},\ \psi(\eta) = \dfrac{N - N_\infty}{N_w - N_\infty},\ \eta = \sqrt{\dfrac{\Omega}{\upsilon}}\, z. \end{cases} \tag{9}$$

Utilizing equation (9) into (1)–(7), we get the following system:

$$2F + H' = 0, \tag{10}$$

$$F'' - F^2 - F'H + G^2 - \gamma_1(H^2F'' + 2FF'H - 2GG'H) - M^2(F + \gamma_1 F'H) = 0, \tag{11}$$

$$G'' - 2FG - HG' - \gamma_1(H^2G'' + 2FHG' + 2F'HG) - M^2(G + \gamma_1 GH) = 0, \tag{12}$$

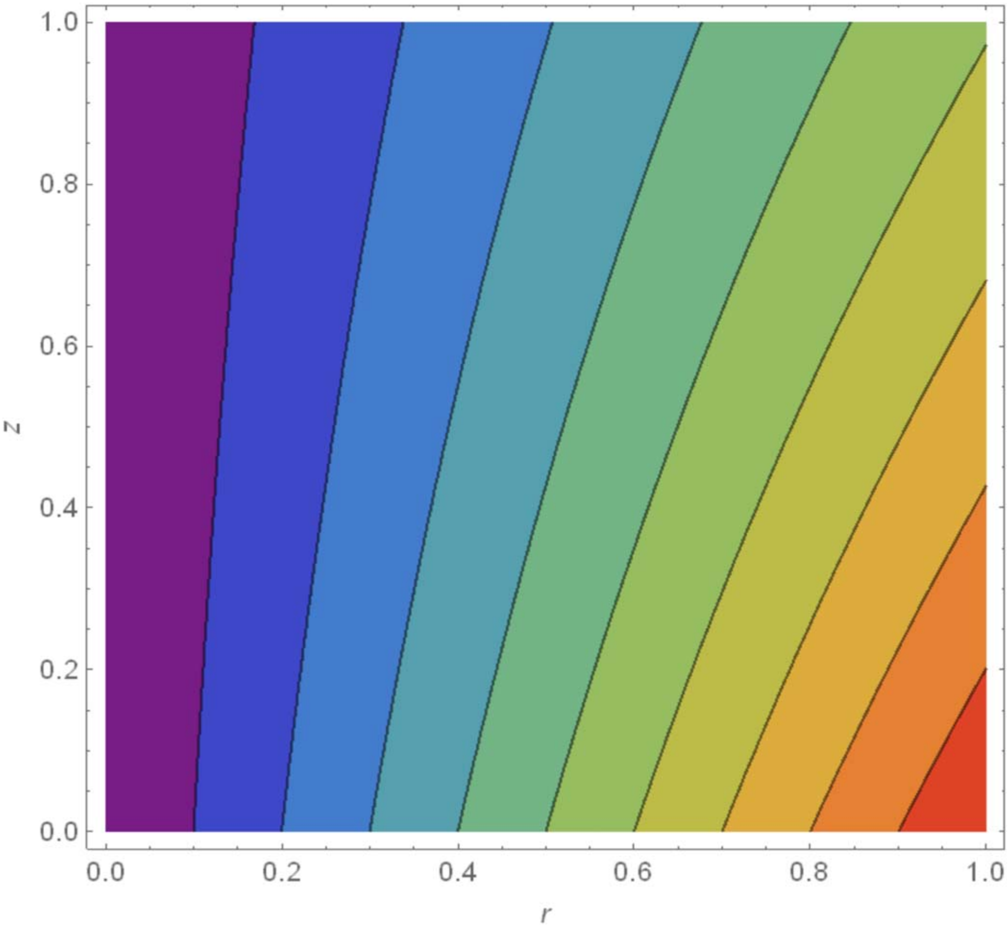

Figure 18. Stream lines for $\Omega = 0.01$.

$$\theta'' - PrH\theta' + PrNb\theta'\phi' + PrNt\theta'^2 - \gamma_2 Pr(HH'\theta' + H^2\theta'') = 0, \tag{13}$$

$$\phi'' - LeH\phi' + \left(\frac{Nt}{Nb}\right)\theta'' - \gamma_3 Le(HH'\phi' + H^2\phi'') = 0, \tag{14}$$

$$\psi'' - L_b H\psi' - P_{e\,b}(\psi'\phi' + \phi''(Ng + \psi)) = 0. \tag{15}$$

The boundary conditions (8) under equation (9) become:

$$\begin{cases} F(0) = \Omega_1,\, G(0) = 1,\, H(0) = 0,\, \theta(0) = 1, \\ \phi(0) = 1,\, \psi(0) = 1 \text{ at } z = 0, \\ F(\infty) \to 0,\, G(\infty) \to 0,\, \theta(\infty) \to 0,\, \phi(\infty) \to 0, \\ \psi(\infty) \to 0 \text{ as } z \to \infty, \end{cases} \tag{16}$$

where

$$M^2 = \sqrt{\frac{\sigma_e \beta_0^2}{\rho\,\Omega}},\, \gamma_1 = \Omega\lambda_1,\, Pr = \frac{\upsilon}{\alpha},\, Nt = \frac{\tau D_T}{\upsilon T_\infty}(T_w - T_\infty),$$

$$Nb = \frac{\tau D_B}{\upsilon}(C_w - C_\infty),\, \gamma_2 = \Omega\tau_0,$$

$\gamma_3 = \Omega\tau_1$, $Le = \frac{\upsilon}{D_B}$, $L_b = \frac{\upsilon}{D_n}$, $P_{eb} = \frac{bW_c}{D_n}$, $Ng = \frac{N_\infty}{N_w - N_\infty}$ and $\Omega_1 = \frac{c}{\Omega}$ stands for magnetic parameter, Deborah number, Prandtl number, thermophoretic constraint, Brownian movement factor, thermal relaxation time constraint, concentration relaxation time constraint, Lewis number, bio-convected Lewis number, bio-convected Peclet number, micro-organisms concentration difference factor and the stretching constraint.

3. Numerical procedure

The finalized equations (10)–(15) under appropriate conditions (16) are solved via RKF method with shooting mechanism to acquired numerical solutions. Equations (10)–(15) are of order second in F, G, H, θ, ϕ and ψ, changed into first order under following procedure.

$$\begin{cases} F = f(1),\, F' = f(2),\, G = f(3),\, G' = f(4), \\ H = f(5),\, \theta = f(6),\, \theta' = f(7), \\ \phi = f(8),\, \phi' = f(9),\, \psi = f(10),\, \psi' = f(11). \end{cases} \tag{17}$$

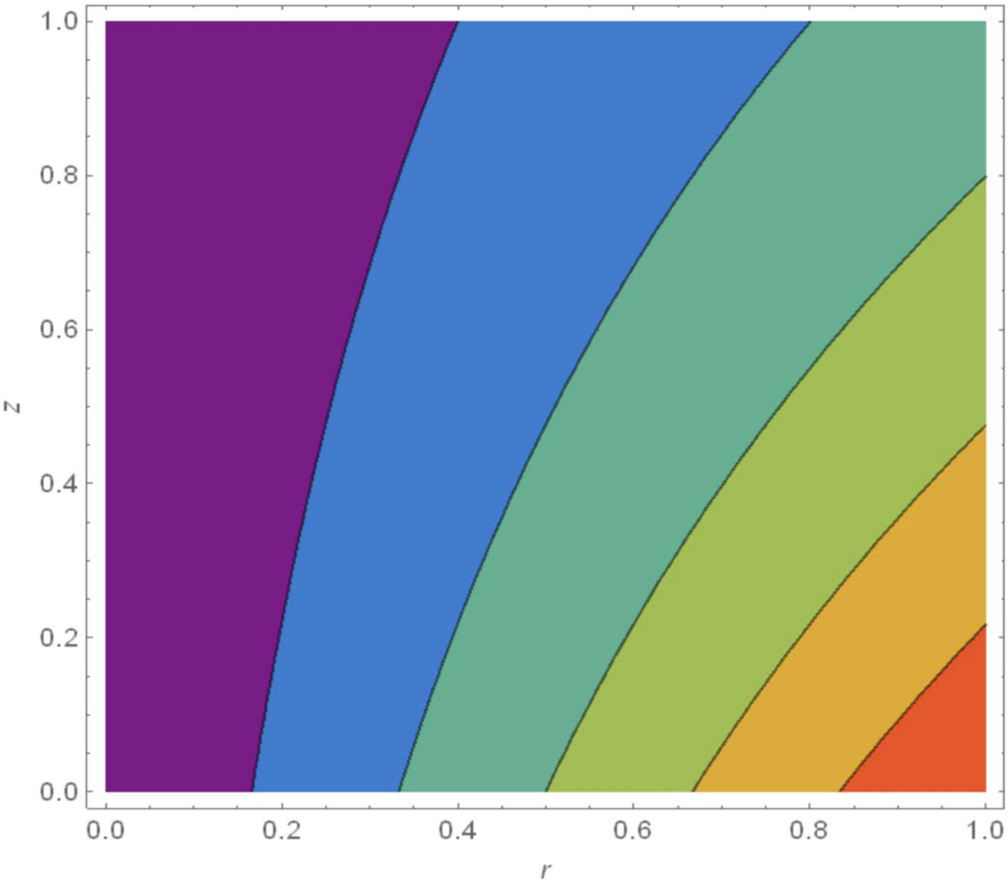

Figure 19. Stream lines for $\Omega = 0.1$.

$$F'' = \frac{1}{1 - \gamma_1(f(5)^2)}\left(\begin{pmatrix} f(1)^2 + f(2)f(5) - (f(3)^2) \\ +(2M^2 f(1) + \gamma_1 f(2)f(5)) \\ +\gamma_1(2f(1)f(2)f(5) \\ -2f(3)f(4)f(5)) \end{pmatrix}\right), \tag{18}$$

$$G'' = \frac{1}{1 - \gamma_1(f(5)^2)}\left(\begin{pmatrix} 2f(1)f(3) + f(4)f(5) \\ +\gamma_1(2f(1)f(4)f(5) \\ +2f(3)f(2)f(5)) \\ +(M^2 f(3) + \gamma_1 f(3)f(5)) \end{pmatrix}\right), \tag{19}$$

$$H' = -2f(1), \tag{20}$$

$$\theta'' = \frac{1}{(1 - \gamma_2 Pr(f(5)^2))}\begin{pmatrix} (Prf(5)f(7) \\ -PrNbf(7)f(9) \\ -PrNt(f(7)^2) \\ (-\gamma_2 Pr(2f(1)f(5)f(7))) \end{pmatrix}, \tag{21}$$

$$\phi'' = \frac{1}{(1 - Le\gamma_3(f(5)^2)))}\begin{pmatrix} Lef(5)f(9) \\ -2Le\gamma_3 f(1)f(5)f(9) \\ -(Nt/Nb)\theta'' \end{pmatrix}, \tag{22}$$

$$\begin{aligned}\psi'' &= L_b f(5)f(11) - P_{eb}(f(9)f(11) \\ &+\phi''(Ng + f(10))),\end{aligned} \tag{23}$$

and the relating boundary restrictions are transfomred into:

$$\begin{cases} f_a(1) = 1, f_a(3) = 1, f_a(5) = 0, f_a(6) = 1, \\ f_a(8) = 1, f_a(10) = 1 \text{ as } z \to 0, \\ f_b(1) = f_b(3) = f_b(6) = f_b(8) = f_b(10) \text{ as } z \to \infty. \end{cases} \tag{24}$$

To resolve the equations (18)–(23), intially, we guess the values of $f(2)$, $f(4)$, $f(5)$, $f(7)$, $f(9)$, $f(11)$, which are absent at initial conditions. After attaining required initial conditions, the equations (18)–(23) are integrated via RKF numerical scheme. The step length in successive iterations is taken 0.001.

4. Graphical description

The impact of notable pertinent flow parameters such as magnetic parameter, velocity ratio parameter M, thermophoretic constraint Nt, Prandtl number Pr, Brownian motion Nb, thermal relaxation time γ_2, concentration relaxation time γ_2, Lewis number Le, bioconvection Lewis number L_b, bioconvection Peclet number P_{eb}, microorganisms concentration difference Ng and the stretching parameter Ω_1 on the flow,

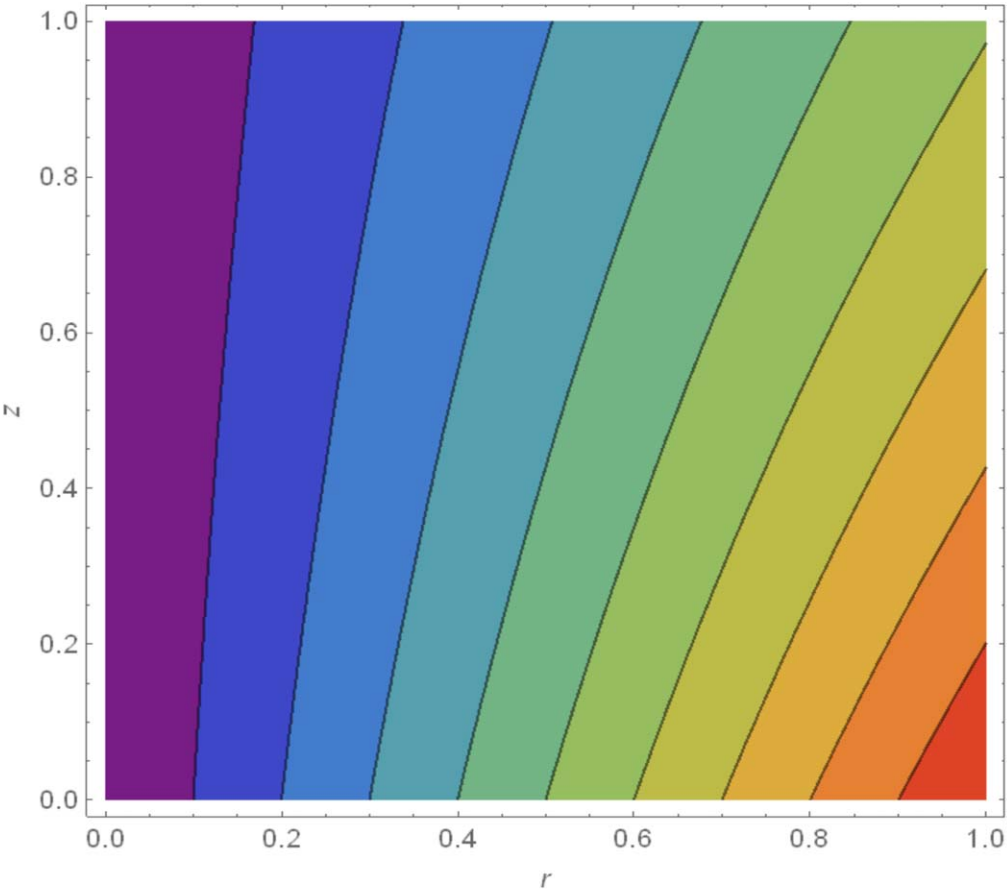

Figure 20. Stream lines for $\gamma_1 = 0.1$.

heat, mass and motile microorganism profiles are illustrated through figures 2–21.

Figures 2 and 3 exhibit that the magnitude of the velocity profiles F and G decreases for boosting values of magnetic constraint M in radial and azimuthal directions, respectively. The exhibition of Lorentz force opposes flow movement in radial direction, therefore the flow velocity reduces due to extra resistance and hence a reduction in radial velocity field is noticed (see figure 2). As the magnetic field is applied in normal direction to rotating disk therefore it resists flow velocity in tangential direction. As a consequence Lorentz force slows down azimuthal velocity field with the increase in magnetic parameter as pictured in figure 3. The velocity curves exponentially decay to zero at short distance from the surface when M is raised. Figures 4 and 5 show the nature of Deborah number γ_1 on F, G. For escalating values of γ_1 velocity profiles decline. In fact, the relaxation time factor is improved by the increasing Deborah number that results in weaker velocities curves. Figure 6 signifies the Prandtl number importance. As Prandtl number contributes to material property which differs from one fluid to another. Smaller thermal conductivity with larger viscosity impart to higher Prandtl number. Therefore, the increased in Pr corresponds to reduction in thermal curves.

Figure 7 exhibits that the curves of temperature field enhances with increment in Nt values. The similar phenomenon is attained against Brownian motion parameter which is shown in figure 8. Significance of thermal field distribution for distinct γ_2 values is predicted in figure 9. It is noticed as the thermal profile is a depreciating activity for rising γ_2. In addition to that the thickness of the thermal boundary layer is declined generally for modified γ_2. The particles of the object need long time to shift heat to its neighborhood particles. Especially, we can declare for large values of γ_2, material represents a non-conducting attitude that is an important in minimization of thermal profile.

The depiction of concentration profiles for bigger Lewis number values are exhibited through figure 10. As Lewis number defines momentum and mass diffusivities ratio so whenever convection of mass diffusion and momentum processes exist, Lewis number is used to characterize the fluid flows. It associates hydrodynamic relative thickness layer and boundary layer of mass transportation. Raising the values of Le elucidates strong molecular movements which ultimately enhance the fluid temperature. Fluid with higher Lewis number contains weaker coefficient of Brownian-diffusion which presents particles to diffuse enormously into fluid. Due to this reason, shorter penetration depth of temperature exists

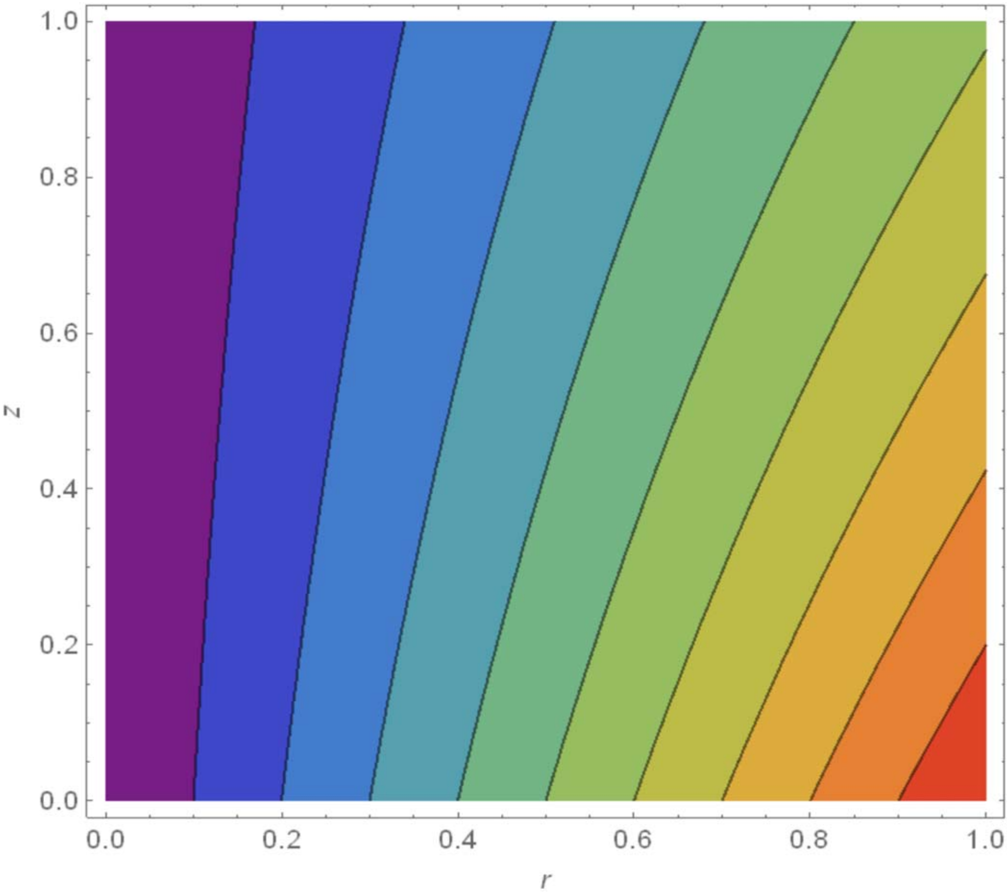

Figure 21. Stream lines for $\gamma_1 = 0.5$.

Table 1. Numerical values of $F'(0)$, $-G'(0)$ and $-\theta'(0)$ for $Pr = 0.71$ and $\gamma_1 = \gamma_2 = Nt = Nb = \Omega_1 = 0$.

M	$F'(0)$ [38]	Present	$-G'(0)$ [38]	Present	$-\theta'(0)$ [38]	Present
0	0.510186	0.510184	0.61589	0.61586	0.32760	0.32761
1	0.309237	0.309236	1.06907	1.06906	0.14667	0.14669
4	0.165701	0.165698	2.01027	2.01024	0.02906	0.02909

in case of larger Lewis number. It illustrates that the concentration profile declines as the Lewis number increases.

The variation in concentration profiles with the Brownian motion parameter is elucidated in figure 11. Reduction in concentration profiles is noticed with the growing values of Nb. Thermophoresis parameter intensifies the concentration profile declines. This nature is clearly shown in figure 12. Figures 13–15 report that the escalating values of Peclet number P_{eb}, and bio convection Lewis number L_b create reduction in motile microorganism and this trend is reverse for the microorganism concentration difference parameter N_g. Patterns which relate to stream lines are sketched via figures 16–21 in order to have clear picture of flow phenomenon. Increased variations in M, Ω_1, and γ_1 resulted into definite curve that obtained by tracing the fluid particle along x-direction under the existence of surface. Furthermore, it is clear that the there is a retardation in the flow pattern. For the validity of our numerical procedure, a comparison of numerical values in limiting scenario is presented through table 1. It is observed that the numerical values have excellent comparison with the literature work [38].

5. Conclusions

Maxwell fluid flow is accounted subject to stretchable rotating disk. Nanofluids Buongiorno model with C–C theories are examined through thermal and concentration constitutive equations. Gyrotactic bio convection features are also incorporated in flow phenomenon. Results are gathered via RKF technique. Following major points are noticed:

- Both the velocity ratio and magnetic parameters declined velocity profiles F and G.
- Thermal field is reduced by Prandtl number while enhanced via thermal relaxation time parameter.

- Nb and Nt have similar impacts on thermal curves however concentration field is affected in opposite ways.
- Bioconvection Lewis and Peclet numbers results into decline of motile organisms rate while the organisms rate is enhanced by Ng.
- Flow pattern signifies retardation along x-direction due by strengthen the stretching parameter.

ORCID iDs

S A Shehzad https://orcid.org/0000-0001-8359-9706
M G Reddy https://orcid.org/0000-0003-2738-3833
A Rauf https://orcid.org/0000-0003-1625-0197

References

[1] Karman T V 1921 Uberlaminare and turbulente Reibung *(ZAMM) Angew. Math. Mech.* **1** 233–52
[2] Cochran W G 1934 The flow due to a rotating disk *Proc. Camb. Phil. Soc.* **30** 365–75
[3] Millsaps K and Pohlhausen K 1952 Heat transfer by laminar flow from a rotating-plate *J. Aeronaut. Sci.* **19** 120–6
[4] Acrivos A, Shah M J and Petersen E E 1960 On the flow of a non-newtonian liquid on a rotating disk *J. Appl. Phys.* **31** 963
[5] Jain M K 1961 The flow of a non-newtonian liquid near a rotating disk *Appl. Sci. Res.* **10** 410
[6] Andersson H I, de Korte E and Meland R 2001 Flow of a power-law fluid over a rotating disk revisited *Fluid Dynam. Res.* **28** 75–88
[7] Attia H A 2007 The effect of ion-slip on the flow of Reiner-Rivlin fluid due to a rotating disk with heat transfer *J. Mech. Sci. Tech.* **21** 174–83
[8] Siddiqui A M, Rana M A and Ahmed N 2008 Effects of hall current and heat transfer onMHD flow of a Burgers' fluid due to a pull of eccentric rotating disks *Commun. Nonlinear Sci. Numer. Simul.* **13** 1554–70
[9] Tabassum M and Mustafa M 2018 A numerical treatment for partial slip flow and heat transfer of non-Newtonian Reiner-Rivlin fluid due to rotating disk *Int. J. Heat Mass Transfer* **123** 979–87
[10] Ahmed J, Khan M and Ahmad L 2019 MHD swirling flow and heat transfer in Maxwell fluid driven by two coaxially rotating disks with variable thermal conductivity *Chin. J. Phys.* **60** 22–34
[11] Turkyilmazoglu M 2012 Effects of uniform radial electric field on the MHD heat and fluid flow due to a rotating disk *Int. J. Eng. Sci.* **51** 233–40
[12] Turkyilmazoglu M 2012 MHD fluid flow and heat transfer due to a stretchingrotatingdisk *Int. J. Therm. Sci.* **51** 195–201
[13] Xun S, Zhao J, Zheng L, Chen X and Zhang X 2016 Flow and heat transfer of OstwalddeWaele fluid over a variable thickness rotating disk with index decreasing *Int. J. Heat Mass Transfer* **103** 1214–24
[14] Shehzad S A, Abbas Z and Rauf A 2019 Finite difference approach and Successive over Relaxation (SOR) method for MHD micropolar fluid with Maxwell-Cattaneo law and porous medium *Phys. Scr.* **94** 115228
[15] Rauf A, Abbas Z and Shehzad S A 2019 Utilization of Maxwell-Cattaneo law for MHD swirling flow through oscillatory disk subject to porous medium *Appl. Math. Mech.* **40** 837–50
[16] Choi S U S 1995 Enhancing thermal conductivity of fluids with nanoparticles *ASME, FED* p 231
[17] Das S K, Putra N, Thiesen P and Roetzel W 2003 Temperature dependence of thermal conductivity enhancement for nanofluids *J. Heat Transfer* **125** 56774
[18] Turkyilmazoglu M 2014 Nanofluid flow and heat transfer due to a rotating disk *Comput. Fluid* **94** 139–46
[19] Hayat T, Khan M I, Alsaedi A and Khan M I 2017 Joule heating and viscous dissipation in flow of nanomaterial by a rotating disk *Int. Commun. Heat Mass Transfer* **89** 190–7
[20] Hayat T, Qayyum S, Khan M I and Alsaedi A 2017 Current progresses about probable error and statistical declaration for radiative two phase flow using $Ag-H_2O$ and $Cu-H_2O$ nanomaterials *Int. J. Hydrog. Energy* **42** 29107–20
[21] Hayat T, Ahmad S, Khan M I and Alsaedi A 2018 Modelling and analyzing flow of third grade nanofluid due to rotating stretchable disk with chemical reaction and heat source *Physica* B **537** 116–26
[22] Ahmad S, Khan M I, Hayat T, Khan M I and Alsaedi A 2018 Entropy generation optimization and unsteady squeezing flow of viscous fluid with five different shapes of nanoparticles *Colloids Surf.* A **554** 197–210
[23] Aziz A, Alsaedi A, Muhammad T and Hayat T 2018 Numerical study for heat generation/absorption in flow of nanofluid by a rotating disk *Results Phys.* **8** 785–92
[24] Mahanthesh B, Gireesha B J, Shehzad S A, Rauf A and Kumar P B S 2018 Nonlinear radiated MHD flow of nanoliquids due to a rotating disk with irregular heat source and heat flux condition *Physica* B **537** 98–104
[25] Sheikholeslami M and Shehzad S A 2018 Simulation of water based nanofluid convective flow inside a porous enclosure via non-equilibrium model *Int. J. Heat Mass Transfer* **120** 1200–12
[26] Acharya N, Bag R and Kundu P K 2019 Influence of Hall current on radiative nanofluid flow over a spinning disk: a hybrid approach *Physica* E **111** 103–12
[27] Mehmood A, Usman M and Weigand B 2019 Heat and mass transfer phenomena due to a rotating non-isothermal wavy disk *Int. J. Heat Mass Transfer* **129** 96–102
[28] Ahmed J, Khan M and Ahmad L 2019 Stagnation point flow of Maxwell nanofluid over a permeable rotating disk with heat source/sink *J. Mol. Liq.* **287** 110853
[29] Fourier J B J 1822 *Theorieanalytique De La chaleur* (Paris)
[30] Hayat T, Qayyum S, Imtiaz M and Alsaedi A 2016 Impact of Cattaneo-Christov heat flux in Jeffrey fluid flow with homogeneous-heterogeneous reactions *PLoS One* **11**
[31] Hayat T, Khan M I, Farooq M, Alsaedi A, Waqas M and Yasmeen T 2016 Impact of Cattaneo-Christov heat flux model in flow of variable thermal conductivity fluid over a variable thicked surface *Int. J. Heat Mass Transfer* **99** 702–10
[32] Mustafa M 2015 Cattaneo-Christov heat flux model for rotating flow and heat transfer of upper-convected Maxwell fluid *AIP Adv.* **5** 047109
[33] Reddy M G 2018 Cattaneo-Christov heat flux effect on hydromagnetic radiative Oldroyd-B liquid flow across a cone/wedge in the presence of cross-diffusion *Eur. Phys. J. Plus* **133** 24
[34] Reddy M G, Rani M V V N L S, Kumar an K G and Prasannakumara B C 2018 Cattaneo-Christov heat flux and non-uniform heat-source/sink impacts on radiative Oldroyd-B two-phase flow across a cone/wedge *J. Braz. Soc. Mech. Sci. Eng.* **40** 95
[35] Abbasi F M and Shehzad S A 2016 Heat transfer analysis for three dimensional flow of Maxwell fluid with temperature

dependent thermal conductivity: application of Cattaneo-Christov heat flux model *J. Mol. Liq.* **220** 848–54

[36] Shehzad S A, Abbasi F M, Hayat T and Alsaedi A 2016 Cattaneo-Christov heat flux model for Darcy-Forchheimer flow of an Oldroyd-B fluid with variable conductivity and non-linear convection *J. Mol. Liq.* **224** 274–8

[37] Ahmed J, Khan M and Ahmad L 2019 Transient thin film flow of nonlinear radiative Maxwell nanofluid over a rotating disk *Phys. Lett.* A **383** 1300–5

[38] Rashidi M M, Abelman S and Mehr N F 2013 Entropy generation in steady MHD flow due to rotating porous disk in a nanofluid *Int. J. Heat Mass Transfer* **62** 515–25